ANNUAL REPORT OF THE ERWIN L. HAHN INSTITUTE FOR MAGNETIC RESONANCE IMAGING

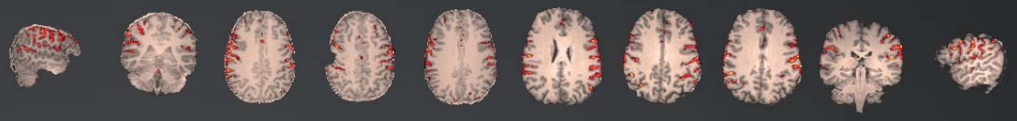

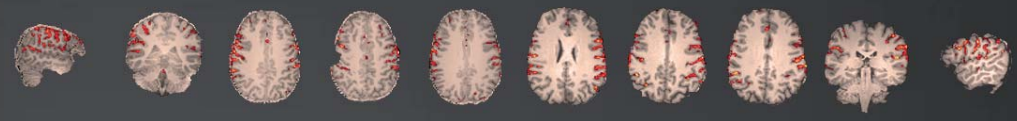

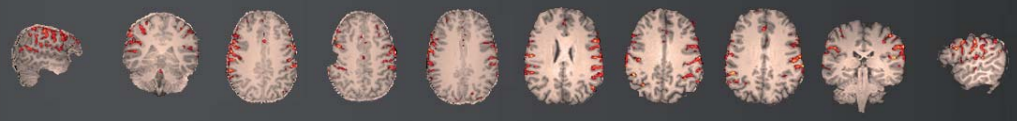

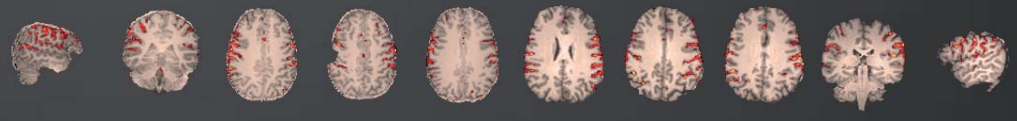

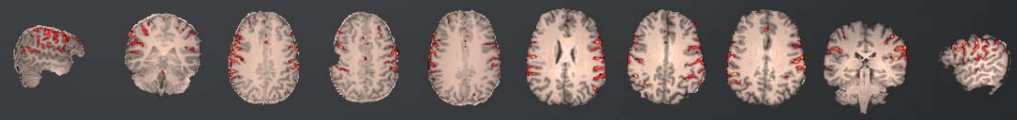

2012

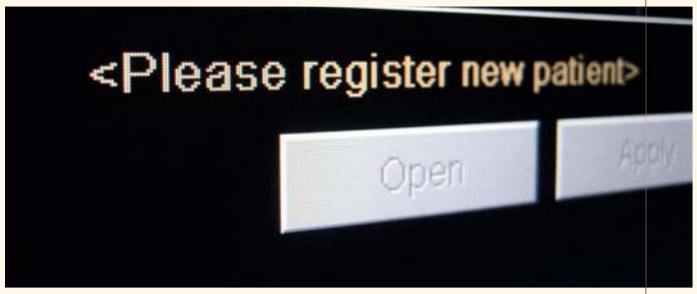

Erwin L. Hahn Institute for Magnetic Resonance Imaging

Arendahls Wiese 199
D-45141 Essen
Germany

t ++49 (0)201-183-6070
f ++49 (0)201-183-6073
w www.hahn-institute.de

Preface

The Erwin L. Hahn Institute has now completed its sixth year of existence, and continues its steady development. 2012 saw the commencement of Mark Ladd's EU advanced grant "MRexcite" which will keep the Institute at the forefront of hardware development for the coming years. In addition considerable technical progress was made in simultaneous multi-slice acquisition techniques, and both spectroscopy and functional MRI remain areas of high activity.
The Institute continued to attract external funding, with participation in the EU-Marie Curie project HiMR and the Helmholtz Alliance project ICEMED.
As ever, a highlight of the year was the annual Erwin L. Hahn lecture, given on this occasion by Prof. Daniel Sodickson of New York University, which was embedded in a highly successful VISTA meeting which attracted over 130 participants mainly from Germany and The Netherlands. The Erwin L. Hahn Institute also developed an ESMRMB workshop on RF simulation motivated by the increasing importance of RF simulations in MRI due to the arrival of ultra-high field MR systems combined with parallel transmission architecture.
The productivity of the Institute remains at a high level, with 20 publications. The staff of the Institute has now grown to such an extent that a problem for the medium term will be in housing them!
I wish you much enjoyment in reading this short report.
David Norris

Essen, January 2013

Anatomical imaging of the prostate at 7T

Optimization of T2-weighted Turbo Spin Echo Imaging of the prostate at 7T

Tom Scheenen

Multiparametric magnetic resonance imaging (mpMRI) plays an increasingly important role in the clinical management of prostate cancer. The workhorse of mpMRI, providing anatomical detail of the prostate as a reference for any other MR-related parameter, is high-resolution T_2-weighted turbo spin echo (TSE) imaging. The potential of 7T for finding new or improving existing MR parameters as additional biomarkers in prostate cancer research and clinical management can only be fully exploited if high-resolution anatomical imaging of the prostate at 7T is a reality. This year, we utilized the existing 8 channel transmit receive array coil setup with B1-shimming and SAR supervision, developed at the Erwin L Hahn Institute, to implement T_2-weighted TSE imaging, and to estimate T_1 and T_2 relaxation times of the prostate and surrounding tissues in a group of healthy volunteers and prostate cancer patients. The results of these measurements were used to define the parameters of a T_2-weighted TSE imaging protocol with consistently high image quality, while allowing full coverage of the prostate gland within RF safety limits.

Nineteen male volunteers (9 healthy with median age 29 years, 10 patients with prostate cancer with median age 66 years) with a median weight of 79 kg (range, 57—100 kg) were included in this study. T1 relaxation times were estimated with a 3D gradient echo progressive saturation experiment, whereas T_2 measurements were performed of a single slice with multiple spin echo sequence. The refocusing pulses of the multi echo and of the TSE sequence were prolonged to reach full refocusing with the available power of the 8-channel TxRx body array coil after B_1-shimming and RF pulse calibration. The mean ± SD maximum achievable B_1+ magnitude after B_1-shimming was 10.6 ± 1.3 μT (derived from 12 subjects).

As expected from T_1-weighted measurements at lower field strengths, no contrast between different prostatic zones was observed in T_1 maps. The mean ± SD T_1 relaxation times in prostate were 1.8 ± 0.2 s in healthy subjects (n=3) and 1.1 ± 0.1 s in patients (n=3). Mean muscle T_1 was 1.3 ± 0.5 s (n=6). In T_2-weighted measurements, anatomical contrast between different tissues in the prostate was visible (Figure 1), and mean ± SD T_2 relaxation times

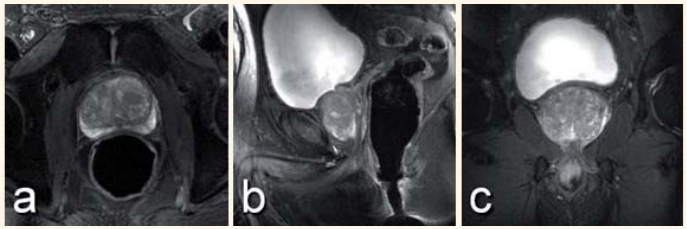

Figure 1: Transversal (a), sagittal (b) and coronal (c) T_2-weighted TSE images of a prostate cancer patient (age 70 years, weight 84 kg). The endorectal receive coil visible in (a) and (b) was tuned to ^{31}P and was therefore not used for signal reception during the acquisition of these images. In (a) the peripheral zone of the prostate is visible as the thin bright rim in the posterior part of the prostate, just above the rectum. All other tissue in this prostate is transition zone tissue.

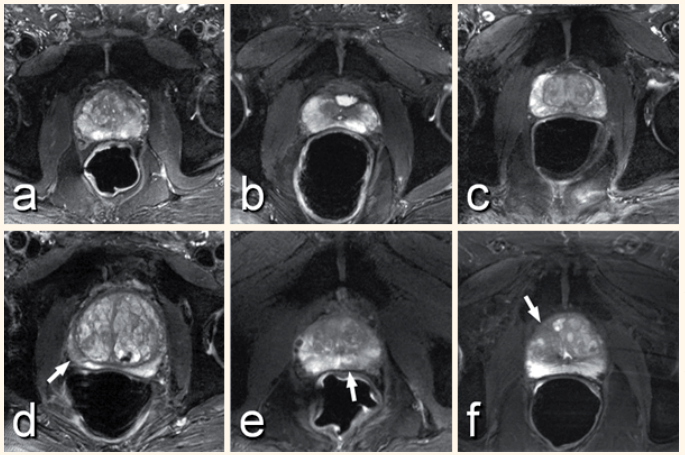

Figure 2: Transversal T_2-weighted TSE images of the prostate midgland (a-d) and apex (e, f) of 6 of the patients included in this study. A good image quality is observed in all images, and no signal voids due to B_1^+ inhomogeneity are observed within the prostate. Note the large differences in size and structure of the different prostates, and low signal intensity from periprostatic lipids in all images. Gold standard histopathology was available in the 3 patients displayed on the bottom row, obtained from radical prostatectomy (d, e) and MR guided biopsy (f). Prostate cancer foci with Gleason Scores of 3+4 (d), 3+3 (e) and 4+4 (f) are indicated by the arrows.

in peripheral zone, transition zone and muscle in healthy subjects were 73.1 ± 16.6, 55.6 ± 6.9 and 31.1 ± 2.3 ms, respectively (n=9), whereas patients (n=6) had values of 120.4 ± 42.8 and 46.2 ± 11.0 ms, respectively. T_2-weighted TSE imaging at an echo time of 71 ms was performed in all subjects. Excellent anatomical detail within the prostate gland and surrounding tissues was obtained, illustrated in Figures 1 and 2.

T_2s were significantly longer and T_1s were shorter in patients than in healthy subjects, although our subject population was too small to draw any definitive conclusions. We speculate that these effects are age related, as the healthy subjects were considerably younger than the patients (median ages 29 and 66 years, respectively), and prostate size, shape and occurrence change with age. Both the shorter T_1 and the longer T_2 relaxation times in patients are beneficial to the SNR of T_2w TSE imaging of prostate cancer patients.

T_2 weighted TSE imaging is particularly SAR intensive because it relies on a large number of refocusing pulses per unit time. At 7T this could limit the number of slices that can be acquired in a multi-slice experiment. The RF power deposited per TSE slice was noted in 6 patients and amounted to 1.0 ± 0.1 W, corresponding to a maximum achievable number of consecutive TSE slices of 31.3 ± 3.7 (minimum 28). This was sufficient for full coverage of the prostate with 3 mm transverse slices with 0.6 mm slice gaps in all patients examined in this study. Full coverage in the other two orthogonal orientations was equally achievable; however, a waiting time between TSE acquisitions was necessary in some cases to allow sufficient dissipation of RF induced heat.

In conclusion, we demonstrated that high quality T_2-weighted TSE imaging of the prostate can be achieved consistently and safely in prostate cancer patients at a magnetic field strength of 7T, providing the essential anatomical detail to new and improved functional (spectroscopic) imaging methods at 7T that are the subject of our ongoing investigations.

More precise imaging of brain activity using T2-weighting at 7 Tesla

Peter Koopmans
Rasim Boyacioglu

Tackling RF power deposition problems using PINS
A study on neural correlates of the perception of bittersweet film clips using 7T fMRI

One of the main benefits of 7 Tesla imaging is that it enables higher resolution acquisitions compared to low-field scanners. In fMRI some of this high precision benefit is lost as with conventional fMRI methods, the T_2^*-weighting biases towards 'activation signals' in draining veins that can be up to a centimetre away from the true site of neuronal activity. Early in the history of BOLD fMRI however, it was shown that T_2-weighted fMRI at high field strengths should be more accurate than T_2^*-weighted methods. The goal is thus to develop a T_2-weighted functional imaging method that is fast enough to satisfy fMRI demands.

The challenge

The biggest technological challenge posed by T_2-weighted imaging (from now on referred to as spin-echo (SE) imaging) at high field strengths is dealing with patient safety. The RF pulses that create spin-echoes use a lot of power, which can lead to tissue heating. Safety regulations prescribe that one should not deposit more RF energy within a certain time window than the body can cope with in terms of cooling: we only allow a rise in temperature of 1° Celsius, i.e. a very mild fever that we know the body is perfectly capable of dealing with. The energy deposition becomes a problem at high field as RF power scales with field strength. At 7 Tesla, the constraint on RF power results in very slow SE protocols as after each RF pulse we have to wait until we can transmit the next one. This severely limits the number of slices one can acquire per unit time and therefore is incompatible with high-resolution fMRI where we need to scan many slices covering the entire brain in less than three seconds.

The solution

A recent invention to accelerate MR imaging is a technique called Simultaneous Multi-Slice (SMS) imaging: instead of scanning all slices sequentially, one can scan multiple slices at the same time, greatly accelerating the process. The downside of the technique is that it uses RF pulses of which the power increases with the acceleration factor. This means that if we acquire four slices at the same time (and could in principle scan four times as fast); the four-fold increase in power deposition would demand us to scan four times as slow, completely cancelling all benefit. At the Erwin L. Hahn institute, we have recently developed a method that creates multislice RF pulses without the associated increase in RF power. This method is dubbed Power Independent of the Number of Slices (PINS) and allowed us to perform the first ever high-resolution, whole brain SE-fMRI study at 7 Tesla.

Results

Figures 3 and 4 show some of the exciting results of this work. Figure 3 shows the brain's resting state activity of the motor network of two subjects. Note how well the BOLD signal pattern is co-localized with the grey matter where the neuronal activity takes place. Figure 4 shows another benefit of T_2 versus T_2^* weighted imaging: it does not suffer from signal voids in areas close to air-tissue interfaces (mostly on the lower frontal parts of the brain near, amongst others, the nasal cavities). T_2^* imaging is very sensitive to the magnetic field perturbation near these interfaces and hence the frontal networks displayed in Figure 4 are seldom found in T_2^*-weighted studies.

Conclusion and outlook

This study has shown the benefit of PINS pulses to accelerate 7 T sequences that would otherwise have been too time-consuming to execute. We have demonstrated its use in SE-fMRI and have shown improved results compared to what has been done in conventional fMRI work. In clinical imaging the spin-echo is the workhorse of MR because of its robustness against artefacts. The PINS method significantly improves the compatibility of spin-echoes with high field strengths and we are therefore currently exploring other promising high-field applications.

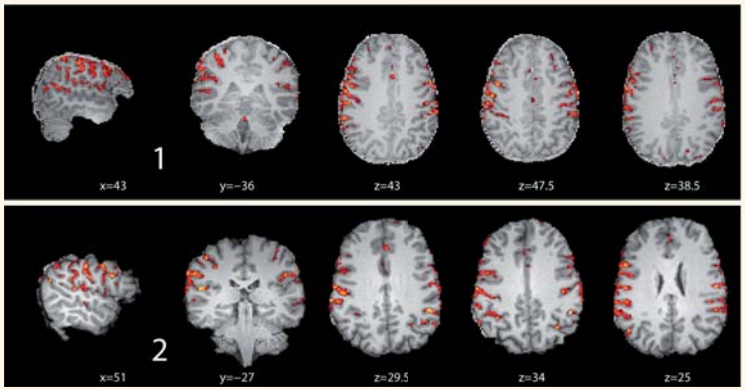

Figure 3: Resting state activity in the motor networks of two volunteers. Note the excellent co-localization of the patterns with the grey matter

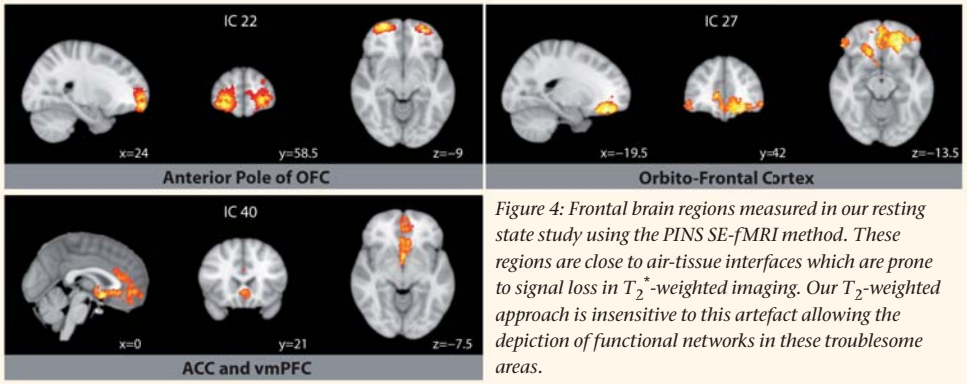

Figure 4: Frontal brain regions measured in our resting state study using the PINS SE-fMRI method. These regions are close to air-tissue interfaces which are prone to signal loss in T_2^*-weighted imaging. Our T_2-weighted approach is insensitive to this artefact allowing the depiction of functional networks in these troublesome areas.

Functional Brain Imaging

Do we empathize with robots? A study on neural correlates of emotional reactions and empathy towards robots using 7T fMRI

Astrid Rosenthal-von der Pütten

Anecdotal evidence suggests that people respond emotionally towards robots and even show signals of social bonding (e.g. [1]). However, research systematically investigating how, when, under what circumstances and to what extent people react emotionally towards robots is scarce. In a previous experiment [7] especially investigating emotional responses towards robots using psychophysiology and self-report we found that participants indeed reacted emotionally towards a robot. Against the background of these results and functional imaging studies, which compared brain responses during the perception of humans and robots (e.g. [1]; [3]), we assumed that robot stimuli elicit comparable activation patterns in emotional brain structures like human stimuli, but that empathy-related structures are more activated when watching human-human interactions. Since human-robot interactions are designed to be positive, it is crucial to investigate both: negative and positive empathic concerns. In the present study, we thus investigated the neural correlates of emotional reactions towards robots, and whether these reactions differ from emotional reactions and empathy towards humans.

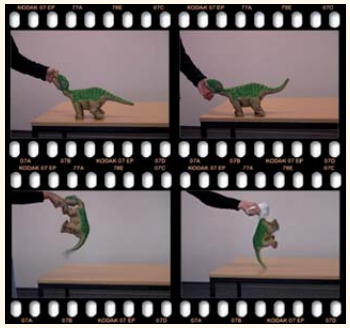

Figure 5: Example scenes from the HRI friendly interaction (feeding, caressing) and the HRI torturing interaction (punching, choking)

Figure 6: Example scenes from the friendly HHI interaction (lean on, hugging) and HHI torturing interaction (choking with plastic bag and rope)

Fourteen healthy volunteers (mean age 23.50 years) participated in the study. We used videos of a robot (Figure 5) and a human (Figure 6) (and as control condition also videos of a box) being treated in a violent and affectionate manner. Based on previous research [5] we hypothesized that compared to the high-level control condition (the box) as well as compared to a low-level control task (a visual search task) participants show different neural activations during the reception of the robot and the human in brain regions involved in emotion processing, regions associated with empathetic reactions and regions activated by cognitive perspective taking (ROI: amygdala, nucleus accumbens, hippocampus; ventromedial prefrontal cortex, dorsomedial prefrontal cortex, secondary somatosensory cortex, anterior cingulate cortex, region of the superior temporal sulcus and parietal lobe). Furthermore, we aimed at exploring whether the perception of the videos involving a human leads to different activation patterns than the perception of the videos involving a robot. Our participants watched six blocks of video clips twice: positive or negative interactions of a human interacting with another human (human-human interaction), a robot (human-robot interaction) or a box (human-box interaction), respectively (cf. Figures 5 and 6 for examples). We acquired functional images on the ELH´s 7 Tesla whole-body scanner (Magnetom 7T, Siemens Healthcare, Erlangen, Germany) using a custom-built 8-channel transmit/receive head coil [6] and an BOLD contrast-sensitive EPI sequence optimized for 7 T functional imaging (also developed at the ELH [7]). General linear models were estimated to test our assumptions. Based on prior hypotheses about key brain areas involved we conducted region-of-interest (ROI) analyses (see above).

The results indicate that there were significant differences in the activation pattern between the low-level control task (visual search task) and all three experimental groups (human-human, human-robot, human-box interaction > low-level control task) predominantly in midbrain and limbic areas. This finding indicates that our manipulation was successful in inducing emotionally relevant situations. Comparing the human-human interaction and human-robot interaction with the human-box interaction condition we found activation differences in the left inferior frontal gyrus. However, our data showed no differences in brain activation when comparing all human-human interaction videos and human-robot interaction videos. This result indicates that both interactions might be equally emotionally relevant. But when comparing only the negative interaction video sets (negative human-human interaction > negative human-robot interaction) we found higher neural activation in the right limbic lobe during the human-human interaction videos (Figure 7). Participants thus seem to show more empathy with a human in a negative situation compared to a robot in a negative situation.

Figure 7: Results of the contrast negative human-human interaction > negative human-robot interaction at a threshold of p = .001 (uncorrected). The right limbic lobe was significantly activated.

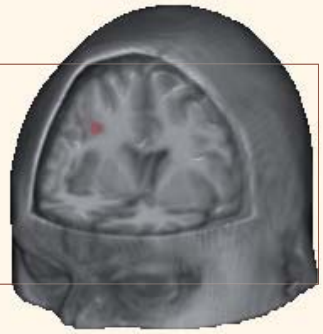

In this project the chair of Social Psychology: Media and Communication at University Duisburg- Essen (Prof. Dr. Nicole Krämer) cooperated with the chair of General Psychology: Cognition (Prof. Dr. Matthias Brand).

References:

[1] von der Pütten AM, et al.: ICMI, 2011 #327.
[2] Rosenthal-von der Pütten AM, et al.: International Journal for Social Robotics, 2013.
[3] Chaminade T, et al.: PLoS ONE, 2010: e11577 EP.
[4] Gazzola V, et al.: NeuroImage, 2007: 1674–1684.
[5] Hein G & Singer T: Current Opinion in Neurobiology, 2008: 153–158.
[6] Orzada S, et al.; ISMRM, 2009: #3010.
[7] Poser BA, et al.; NeuroImage, 2009: 1162-72.

Intracranial MR Imaging

Sören Johst

Time-of-Flight MR Angiography at 7 T using Venous Saturation Pulses with Reduced Flip Angles

It has been shown that time-of-flight (TOF) MR angiography (MRA) highly profits from increased field strengths [8]. In TOF MRA sequences, repetition intervals TR are chosen preferably as short as possible to take advantage of the prolonged relaxation values T_1 at 7 T. As the high-resolution 3D datasets are acquired over many excitation cycles, excellent suppression of static background tissue can easily be achieved when using short TR. In comparison, the signal from inflowing, completely relaxed blood is high, providing the desired image contrast for high-resolution depiction of the arterial vasculature.

The application of saturation pulses for suppression of the venous system using a standard flip angle of 90° is often not possible without substantial prolongation of TR. Using the variable rate selective excitation (VERSE) algorithm for excitation / saturation RF pulses, the use of 90° saturation pulses is possible, but still TR has to be prolonged to stay within specific absorption rate (SAR) limits and thus avoid tissue heating [9, 10]. In this work, we proposed to take advantage of the inherent saturation effects of the relative short TR in this type of sequence not only for background suppression but also for the saturation of the venous system.

To achieve this, three different changes were introduced beyond the utilization of VERSE. 1) Shorter saturation pulses (which allow shorter TR) are applied to suppress an area above the imaging slab that is as thick as possible and which covers the superior sagittal sinus. As a slice-selection gradient controls the thickness of the saturation area, changes in duration (and thus changes in the frequency bandwidth of the pulse) are balanced by the amplitude of this gradient. 2) To remain in conformance with SAR limits, the shorter saturation RF pulses are applied with smaller flip angle. 3) Not only the duration of the RF pulse itself prolongs the minimum TR, but also the spoiler gradients which follow the saturation pulse. Therefore, we also implemented spoiler gradients with shorter duration.

In this work, we examined the influence of different saturation pulse durations on the excitation profile of a 3D TOF MRA sequence with the constraint of minimizing total measurement time, and systematically varied the flip angle of the saturation pulses (α_{SAT}) with the aim of achieving sufficient suppression of venous signals inside the imaging slab, with α_{SAT} as small as possible to ameliorate SAR limitations.
A slab covering the Circle of Willis – considered to be the most clinically relevant intracranial vascular territory – was chosen for the saturation flip angle variation scans. The best value for α_{SAT} was ascertained in 7 healthy volunteers. As the normally used parameter range in 7 T TOF MRA covers TR $\in$ [20 ms, 35 ms] and $\alpha \in$ [15°, 35°], the saturation flip angle α_{SAT} was varied for $\alpha \in$ [15°, 35°] and TR = 20 ms. The thereby determined α_{SAT} was then validated for TR up to 35 ms. The excitation flip angle α was varied in steps of 5° and TR in steps of 5 ms. A vessel-to-background ratio ($VBR = S_{Sinus} / S_{Tissue}$) giving the ratio of the signal in the sagittal sinus to the signal in the surrounding brain tissue was defined to measure the degree of saturation of the sagittal sinus. Although a VBR ≤ 1 would be sufficient to suppress the venous signal in MIPs, the criterion for acceptable venous saturation was set to VBR ≤ 0.6 to account for individual differences e.g. in head shapes and sizes or flow velocity.
For the considered excitation flip angles $\alpha \in$ [15°, 35°], the choice of the most desirable saturation flip angle was determined to be $\alpha_{SAT} = \alpha + 15°$ (Figures 8 and 9). In all volunteer scans, the respective α_{SAT} led to sufficient venous saturation over the entire considered TR range (Figure 10).

This work shows that by reducing the flip angle α_{SAT}, saturation pulses can be applied every TR in high-resolution clinical TOF protocols using a TR as short as 20 ms (Figures 11 and 12). This is vital, since the total acquisition time scales directly with TR. Also, by making the duration of the saturation pulses a parameter that can be changed online, more flexibility in protocol creation can be gained. An $\alpha_{SAT} = (\alpha + 15°)$ is sufficient for suppression of the venous system in TOF MRA protocols in the parameter range $\alpha \in$ [15°, 35°] and TR $\in$ [20, 35] ms, which is the range normally used at 7 T. Instead of the standard 90° saturation pulse, only half of this flip angle (or even less) is necessary, substantially ameliorating SAR constraints and enabling acquisition of very high resolution in acceptable imaging time.

For details of this technique see Sören Johst, Karsten H. Wrede, Mark E. Ladd, and Stefan Maderwald. Investigative Radiology, Volume 47, Number 8, August 2012, pp. 445-450.

References:

[8] Maderwald et al. Magma 21:159-167 (2008)
[9] Conolly et al. J Mag Reson 78:440-458 (1988)
[10] Schmitter et al. MRM 68:188-197 (2012)

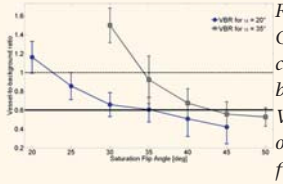

Figure 8: Comparison of the course of vessel-to-background ratio VBR as a function of the saturation flip angle for excitation flip angles α = 20° and 35°. The similarity and the shift toward higher flip angles can be clearly seen. In general, saturation flip angles of less than half of the typically used 90° are sufficient to achieve acceptable venous saturation (VBR ≤ 0.6).

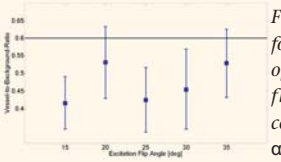

Figure 9: VBR for the variation of the excitation flip angle for corresponding $\alpha_{SAT} = (\alpha + 15°)$ and TR = 20 ms. A saturation flip angle 15° greater than the excitation flip angle is sufficient for adequate venous suppression (VBR ≤ 0.6) in all cases.

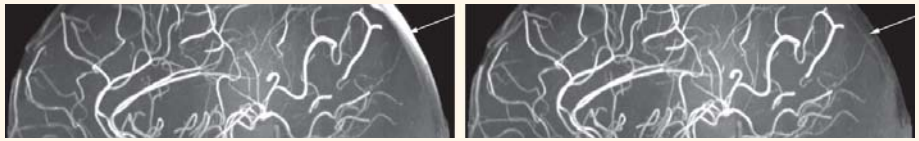

Figure 10: Sagittal MIP with skull removed showing TOF without (top) and with (bottom) venous saturation RF pulse; α_{SAT} = 35° led to complete saturation of the sagittal sinus for α = 20° and TR = 20 ms. White arrows indicate sagittal sinus.

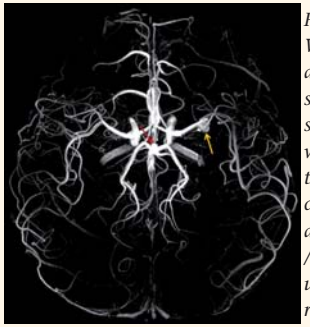

Figure 11: Whole-brain axial MIP with skull removed showing patient with basilar tip and middle cerebral artery aneurysms (red / yellow arrows) using a high-resolution TOF MRA protocol (α_{SAT} = 35°, α = 20°, TR = 20 ms).

Figure 12: Whole-brain axial MIP with skull removed showing patient with arteriovenous malformation (AVM; red arrow) using a high-resolution TOF MRA protocol (α_{SAT} = 35°, α = 20°, TR = 20 ms). Due to the suppression of venous blood inside the sagittal sinus, the drainage of hyperintense arterial blood into the lower part of the sagittal sinus can clearly be seen.

6th Erwin L. Hahn Lecture

Virtual institute meets institute


The audience


The lecture: Unexpected Tomography: From Magnetic to Electrical Imaging with MRI


The 1st Erwin L. Hahn Institute Award for Young Scientists


The location: The red dot museum


Time for discussions


And finally some drinks

Current Grants

Timmann D, Cerebellar-Cortical Control: Cells, Circuits, Computation and Clinic. Marie Curie Initial Training Grant, EU; duration 4 years (January 2010 – December 2013)

Scheenen T, Exploring the aggressiveness of prostate cancer to enable an individualised treatment approach. European Research Council; duration 5 years (March 2010 – February 2015)

Ladd ME, Rennings A, Solbach K. Competition Science-to-Business PreSeed: MetaCoils – Metamaterial-based high-frequency-coils for 7-Tesla-MRI; duration 3 years (July 2010 – April 2012)

Brand M, Wolf OT. Stress und Risikoentscheidungen – behaviorale, neuroendokrine und neurale Korrelate der Interaktion von Stress, exekutiven Funktionen und Entscheidungen in Risikosituationen; duration 2 years (October 2010 – September 2012)

Solbach K, Rennings A. Investigation of coil concepts based on flat Electronic Band Gap (EBG) structures for use in magnetic resonance imaging (MRI). German Research Foundation; duration 2 years (January 2011 – December 2012)

Norris D, Tegenthoff M. modulation of inhibitory cortical mechanisms measured using GABA MRS at 7 Tesla. MERCUR; duration 2 years (January 2011 – December 2012)

Timmann D, Ladd ME. Contribution of the human cerebellum to extinction learning and renewal, Project in the Research Unit FOR 1581; German Research Foundation; duration 3 years (January 2011 – December 2013)

Ladd ME, MRexcite: Unlocking the potential of ultra-high-field MRI through manipulation of radiofrequency excitation fields in human tissue. European Research Council, duration 5 years (May 2012 – April 2017)

Norris D, Tendolkar, Wiltfang et.al., Imaging and Curing Environmental Metabolic Diseases. (ICEMED) Helmholtz-Gesellschaft; duration 5 years (July 2012 – June 2017)

Ladd ME, Norris D, et.al., HiMR: Ultra-High Field Magnetic Resonance Imaging. Marie Curie Actions - Initial Training Networks, EU; duration 4 years (November 2012 - October 2016)

Personnel

New in 2012

M.Sc. Ashraf Abuelhaija
B.Sc. Patricia Ulloa Almendras
Dr. med. Karsten Beiderwellen
M.Sc. Jenni Bersch
M.Sc. Rasin Boyacioglu
Dr. rer. nat. Marcel Gratz
Dipl.-Phys. René Gumbrecht
M.Sc. Michael Kleinnijenhuis
B.Sc. Maike Lindemann
MEng. Ria Pradhan

Left in 2012

M.Sc. Patricia Ulloa Almendras
M.Sc. Mehmet Ramazanoglu
Dr. rer. nat. Hasan Nuzha

Publications

Berghoff, M., Schlamann, M., Maderwald, S., Grams, A., Kaps, M., Ladd, M. E., Gizewski, E. (2012). *7 Tesla MRI demonstrates vascular pathology in Balo's concentric sclerosis.* Multiple sclerosis (Houndmills, Basingstoke, England), [Epub ahead of print]

Dammann, P., Wrede, K. H., Maderwald, S., Hindy, N. E., Mueller, O., Chen, B., Zhu, Y., Hütter, B., Ladd, M. E., Schlamann, M., Sandalcioglu, I., Sure, U. (2012). *The venous angioarchitecture of sporadic cerebral cavernous malformations: a susceptibility weighted imaging study at 7 T MRI.* Journal of neurology, neurosurgery, and psychiatry, [Epub ahead of print]

Goa, P., Poser, B. & Barth, M. (2012). *Modeling and suppression of respiration induced B0-fluctuations in non-balanced steady-state free precession sequences at 7 Tesla.* Magma, [Epub ahead of print]

Grams, A., Kraff, O., Umutlu, L., Maderwald, S., Dammann, P., Ladd, M. E., Forsting, M., Gizewski, E. (2012). *MRI of the lumbar spine at 7 Tesla in healthy volunteers and a patient with congenital malformations.* Skeletal radiology, 41(5), 509-14.

Hoyer, C., Vogt, M., Richter, S., Zaun, G., Zahedi, Y., Maderwald, S., Ladd, M. E., Winterhager, E., Grümmer, R., Gass, P. (2012). *Repetitive exposure to a 7-Tesla static magnetic field of mice in utero does not cause alterations in basal emotional and cognitive behavior in adulthood.* Reproductive toxicology (Elmsford, N.Y.), 1(34), 86 - 92.

Johst, S., Wrede, K. H., Ladd, M. E. & Maderwald, S. (2012). *Time-of-Flight Magnetic Resonance Angiography at 7 T Using Venous Saturation Pulses With Reduced Flip Angles.* Investigative radiology, 8(47), 445-50.

Kobus, T., Bitz, A. K., van Uden, M., Lagemaat, M., Rothgang, E., Orzada, S., Heerschap, A., Scheenen, T. (2012). *In Vivo (31) P MR spectroscopic imaging of the human prostate at 7 T: Safety and feasibility.* Magnetic resonance in medicine, 68(6), 1683-95.

Koopmans, P., Boyacioğlu, R., Barth, M. & Norris, D. G. (2012). *Whole brain, high resolution spin-echo resting state fMRI using PINS multiplexing at 7T.* NeuroImage, 3(62), 1939 - 46.

Küper, M., Thürling, M., Stefanescu, R., Maderwald, S., Roths, J., Elles, H., Ladd, M. E., Diedrichsen, J., Timmann, D. (2012). *Evidence for a motor somatotopy in the cerebellar dentate nucleus-an fMRI study in humans.* Human brain mapping, 33(11), 2741-9.

Maderwald, S., Thürling, M., Küper, M., Theysohn, N., Müller, O., Beck, A., Aurich, V., Ladd, M. E., Timmann, D. (2012). *Direct visualization of cerebellar nuclei in patients with focal cerebellar lesions and its application for lesion-symptom mapping.* NeuroImage, 63(3), 1421-31.

Moser, E., Stahlberg, F., Ladd, M. E. & Trattnig, S. (2012). *7-T MR-from research to clinical applications?.* NMR in biomedicine, 5(25), 695 - 716.

Orzada, S., Johst, S., Maderwald, S., Bitz, A. K., Solbach, K. & Ladd, M. E. (2012). *Mitigation of B(1) (+) inhomogeneity on single-channel transmit systems with TIAMO.* Magnetic resonance in medicine, [Epub ahead of print]

Orzada, S., Maderwald, S., Poser, B., Johst, S., Kannengiesser, S., Ladd, M. E., Bitz, A. K. (2012). *Time-interleaved acquisition of modes: An analysis of SAR and image contrast implications.* Magnetic resonance in medicine, 67(4), 1033-41.

Solbach, K., Yazdanbakhsh, P. & Bitz, A. K. (2012). *Variable power combiner for RF mode-shimming in 7 Tesla MR Imaging.* IEEE transactions on bio-medical engineering, 9(59), 2549 - 57.

Steinseifer, I., Wijnen, J., Hamans, B., Heerschap, A. & Scheenen, T. (2012). *Metabolic imaging of multiple X-nucleus resonances.* Magnetic resonance in medicine, [Epub ahead of print]

Thürling, M., Hautzel, H., Küper, M., Stefanescu, M., Maderwald, S., Ladd, M. E., Timmann, D. (2012). *Involvement of the cerebellar cortex and nuclei in verbal and visuospatial working memory: A 7 T fMRI study.* NeuroImage, 3(62), 1537 - 50.

Umutlu, L., Forsting, M. & Ladd, M. E. (2012). *Ultrahigh-field magnetic resonance imaging: the clinical potential for anatomy, pathogenesis, diagnosis and treatment planning in neck and spine disease.* Neuroimaging clinics of North America, 2(22), 363-71.

Umutlu, L., Maderwald, S., Kinner, S., Kraff, O., Bitz, A. K., Orzada, S., Johst, S., Wrede, K. H., Forsting, M., Ladd, M. E., Lauenstein, T., Quick, H. (2012). *First-pass contrast-enhanced renal MRA at 7 Tesla: initial results.* European radiology, [Epub ahead of print]

Umutlu, L., Maderwald, S., Kraff, O., Kinner, S., Schäfer, L., Wrede, K. H., Antoch, G., Forsting, M., Ladd, M. E., Lauenstein, T., Quick, H. (2012). *New look at renal vasculature: 7 tesla nonenhanced T1-weighted FLASH imaging.* Journal of magnetic resonance imaging, 3(36), 714 - 21.

Wrede, K. H., Johst, S., Dammann, P., Umutlu, L., Schlamann, M., Sandalcioglu, I., Sure, U., Ladd, M. E., Maderwald, S. (2012). *Caudal Image Contrast Inversion in MPRAGE at 7 Tesla Problem and Solution.* Academic radiology, 2(19), 172-8.

Erwin L. Hahn Institute for Magnetic Resonance Imaging

Arendahls Wiese 199
D-45141 Essen
Germany

t ++49 (0)201-183-6070
f ++49 (0)201-183-6073
w www.hahn-institute.de

Graphic design
AMP Studio, Duisburg

Photography

PARTICIPATING INSTITUTIONS

FAKULTÄT FÜR
INGENIEURWISSENSCHAFTEN